JACS
JOURNAL OF THE AMERICAN CHEMICAL SOCIETY
Communication
pubs.acs.org/JACS

Negative Linear Compressibility of a Metal–Organic Framework

Wei Li,[†] Michael R. Probert,[§] Monica Kosa,*[,‡] Thomas D. Bennett,[†] A. Thirumurugan,[†] Ryan P. Burwood,[†] Michele Parinello,[#] Judith A. K. Howard,[§] and Anthony K. Cheetham*[,†]

[†]Department of Materials Science and Metallurgy, University of Cambridge, Cambridge CB2 3QZ, United Kingdom
[§]Department of Chemistry, Durham University, Durham DH1 3LE, United Kingdom
[‡]Faculty of Exact Sciences, Department of Chemistry, Bar-Ilan University, Ramat-Gan 52900, Israel
[#]Department of Chemistry and Applied Biosciences, ETH Zurich, USI-Campus, Via G. Buffi 13, 6900 Lugano, Switzerland

Supporting Information

ABSTRACT: A 3D hybrid zinc formate framework, $[NH_4][Zn(HCOO)_3]$, possessing an *acs* topology, shows a high degree of mechanical anisotropy and negative linear compressibility (NLC) along its *c* axis. High-pressure single-crystal X-ray diffraction studies and density functional theory calculations indicate that contraction of the Zn–O bonds and tilting of the formate ligands with increasing pressure induce changes in structure that result in shrinkage of the *a* and *b* axes and the NLC effect along *c*.

Most materials contract in all directions under increasing hydrostatic pressure, with only a small number of materials known to expand along a specific direction while undergoing total volume reduction under these conditions.[1] This unique mechanical effect, known as negative linear compressibility (NLC), is remarkably rare but has potential applications in high-pressure environments, such as optical telecommunication lines and sensor systems. For example, NLC materials can exhibit stretch densification along the NLC orientation, a unique trait that is of importance in the development of highly sensitive pressure detectors, robust shock absorbing materials, and 'smart' body armor.[2,3]

Baughman et al. summarized the possible mechanisms for achieving NLC and identified several basic structural motifs that are known to give rise to the phenomenon, such as 'wine-rack' type connectivity.[1] However, only a handful of NLC materials have been discovered thus far, the majority of which are inorganic systems.[1,2] The most well-known examples are $LaNbO_4$,[4] elemental Se,[5] and $BAsO_4$ with the α-cristobalite structure.[6] Goodwin et al. ascribed the remarkably large NLC effect (-5 TPa^{-1}) in the cyanide framework, $Ag_3[Co(CN)_6]$, to the 'wine-rack' motif.[1,2] Very recently, the strongest NLC effect (-12 TPa^{-1}) was discovered in the related framework, $KMn[Ag(CN)_2]_3$, in which the inclusion of extra-framework counterions appears to frustrate the soft phonon modes responsible for destroying NLC.[7] It has also recently been demonstrated that small molecule organic systems can adopt NLC behavior, such as the hydrogen-bonded 'lattice fence' arrangement in methanol monohydrate, giving rise to NLC of -3.8 TPa^{-1}.[8] Direct observation of NLC in inorganic–organic framework materials has not, to the best of our knowledge, been reported to date. However, the linear compressibilities extracted from elastic constant tensors of some hybrid crystals, for example, cesium biphthalate, have been shown to be consistent with this rare phenomenon.[1] Given the immense structural and chemical diversity of hybrid frameworks,[9−11] we anticipate that NLC might be found in such systems. In the present work, we use nanoindentation measurements, single-crystal high-pressure X-ray diffraction studies, and density functional theory (DFT) calculations to demonstrate and explain the mechanism by which a 3D zinc formate framework, $[NH_4][Zn(HCOO)_3]$ (**1**), exhibits significant mechanical anisotropy and NLC along its *c* axis, in the range of 0–1 GPa.

It was previously reported that **1** crystallizes under ambient conditions in the chiral space group $P6_322$ and has a 3D anionic framework structure with NH_4^+ cations situated within the 1D channels formed along the *c* axis (Figure 1a).[12] There is only one C–O bond and one Zn–O bond in the asymmetric unit of **1** due to the symmetry of the system. The NH_4^+ cations are connected to the anionic framework via N–H···O hydrogen bonds, with N···O distances of 2.973(2) Å. Each ZnO_6 octahedron within the anionic framework is connected to six neighboring zinc atoms in a trigonal prismatic mode by *anti–anti* bridging $HCOO^-$ ligands (Figure 1b,c), which gives rise to a uninodal *acs* topology ($4^9{\cdot}6^6$).[13] Each metal node in the ($4^9{\cdot}6^6$) framework topology is thus involved within nine four-membered and six six-membered Zn–OCHO–Zn–OCHO rings.

Nanoindentation measurements were performed using a sharp Berkovich tip (radius ~100 nm) in the continuous stiffness measurement (CSM) mode. The indenter axes were aligned normal to the {002} and {010} orientations of framework **1**. Representative *P*–*h* curves obtained on both facets are shown in Figure 2, and the average values of the elastic moduli (E) and the hardness (H) normal to {002} and {010}, extracted from the *P*–*h* curves, were calculated over depths of 200–1000 nm in order to minimize the imperfection of the Berkovich tip.[14] Though the loading during indentation is not perfectly uniaxial and the stress field generated underneath the indenter is nonuniform, indentation can be used to probe the mechanical properties of single crystals since the measured modulus is strongly dependent on the elastic response along the indenter axis and is weakly affected by the

Received: May 29, 2012
Published: July 3, 2012

dx.doi.org/10.1021/ja305196u | J. Am. Chem. Soc. 2012, 134, 11940–11943

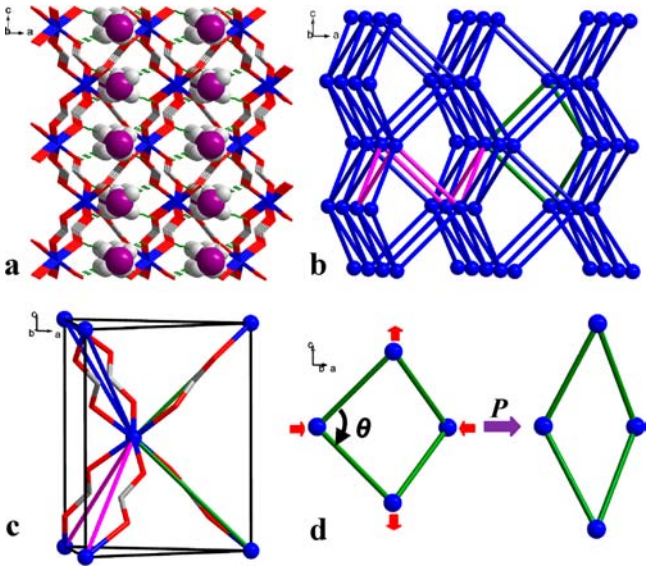

Figure 1. (a) Framework structure of $[NH_4][Zn(HCOO)_3]$, **1**, with ammonium cations situated in the channels, viewed along the *b* axis at ambient pressure. (b) The *acs* topology of framework **1** in which one four-membered and one six-membered Zn−OCHO−Zn−OCHO ring are illustrated in pink and green, respectively, where the balls and sticks represent the Zn atoms and formate ligands. (c) The trigonal prismatic connecting environment of zinc metal nodes in framework **1** (note that the coordination geometry of ZnO_6 unit is octahedral). (d) The schematic compression behavior in response to an increase in pressure, showing the effect on the Zn−Zn connectivity; the Zn−Zn−Zn angle, θ, within the four-membered rings is illustrated. Color scheme: Zn(II), blue; O, red; C, gray; N, purple; H, light gray. N−H···O bonds are represented as dotted green lines. Hydrogen atoms of formate groups are omitted for clarity.

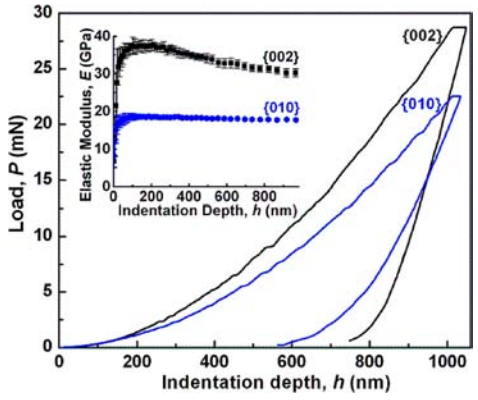

Figure 2. Representative *P*−*h* curves for **1** with {002} and {010} orientated facets measured by a Berkovich tip. Inset: elastic moduli of **1** as a function of indentation depth, wherein each error bar represents the standard deviation from 20 indents.

transverse directions.[15,16] The average elastic moduli normal to the orthogonal facets were found to be $E_{\{002\}}$ = 34.4(9) GPa and $E_{\{010\}}$ = 18.2(2) GPa, which reveals the intrinsic elastic anisotropy of framework **1** with $E_{\{002\}}/E_{\{010\}} \approx 1.9$. The Young's moduli are broadly similar to those of the dense cation−anion type formates, for example, $E \approx 19.0$ GPa for $[(CH_3)_2NH_2][Zn(HCOO)_3]$.[17] It can be seen that the *c* orientation is relatively stiff compared with the *a* and *b* orientations, reflecting the structural anisotropy of the hexagonal framework. Based on the nanoindentation data, we hypothesized that, under hydrostatic compression, the framework would be highly compressible along the *a* and *b* axes but hardly compressible along *c*.

High-pressure single-crystal X−ray diffraction data were collected from ambient pressures to 0.94 GPa at room temperature on a Ag source version of the XIPHOS diffractometer (Tables S1 and S2, Supporting Information (SI)). Pressure was applied using a diamond anvil cell, with paraffin oil as a hydrostatic transmitting medium and ruby fluorescence for pressure calibration.[18,19] The evolution of the change in unit cell volume of **1** as a function of pressure is shown in Figure 3. The volume decreases with increasing

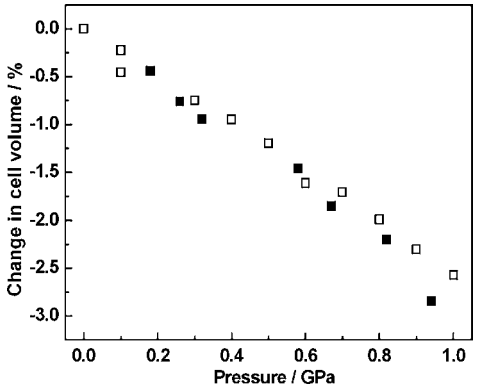

Figure 3. Evolution of the changes of unit cell volume as a function of hydrostatic pressure (experimental data as solid black squares; computational results as open black squares; error bars are smaller than the squares).

pressure, as expected, and the measured percentage of shrinkage is ∼3.0% per GPa in the studied pressure range. The bulk modulus of **1** was estimated by using a second-order Birch−Murnaghan equation of state (EoS), giving a value for K_0 of 32.8(16) GPa (Figure S1, SI).[20−22] This value is significantly higher than those found for several zeolitic imidazolate frameworks[23−27] but comparable with values for the hybrid frameworks HKUST-1[28] and the dense hybrid $[Cu(CO_3)_2][(CH_6N_3)_2]$.[29]

Analysis of the variation of the individual lattice parameters with pressure, shown in Figure 4, reveals the major finding of this work. The empirical fitting $l = l_0 + \lambda(p - p_c)^v$ gives the linear compressibility along *a* as 15.8(9) TPa^{-1}, showing that the *a* and *b* axes are highly compressible as hypothesized[30] (see Figure 4). However, the *c* axis shows a rare example of NLC with a coefficient of −1.8(8) TPa^{-1}. Though previous reports have shown that ZIF-8,[24] HKUST-1,[28] and metal−organic framework (MOF)-5[31] can exhibit volumetric expansion at small initial pressures, in these cases the phenomenon results from an uptake of pressure-transmitting fluids into the MOF cavities and cannot be ascribed to an intrinsic NLC effect of a closed system.[32] The NLC value of −1.8 TPa^{-1} for framework **1** is comparable with values for $BAsO_4$,[4] elemental Se,[5] $Ag_3[Co(CN)_6]$,[6] and methanol monohydrate,[8] but about four times smaller than that of $KMn[Ag(CN)_2]_3$.[7] The ratios of the axial compressibilities to the volume compressibilities are β_a/β_V = 0.52 and β_c/β_V = −0.06.[1,8] A ratio of 0.33 is expected for isotropic materials.

The structural changes of **1** as a function of pressure are quite subtle in the studied range of 0−0.94 GPa. DFT calculations were therefore performed in order to better understand the

dx.doi.org/10.1021/ja305196u | J. Am. Chem. Soc. 2012, 134, 11940−11943

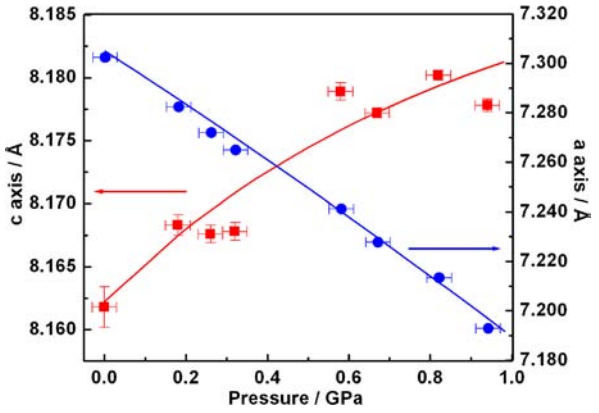

Figure 4. Evolution of the *a* and *c* axes as a function of hydrostatic pressure. The blue (*a* axis) and red (*c* axis) solid lines represent linear compressibilities obtained from an empirical fit $l = l_0 + \lambda(p - p_c)^v$ described in ref 30. Experimental data are shown, with error bars, as blue circles and red squares.

effect of pressure on the framework. The starting model for the computational study was the structure of $[NH_4][Zn(HCOO)_3]$ at ambient pressure. The computational study gives a bulk modulus of 38.1 GPa and the percentage shrinkage of ~2.6% per GPa within the range of 0−1 GPa, which is consistent with the experimental results (Figures 3 and S1, SI). As seen from Table S2, SI, there are no significant changes in the C−O bond lengths or O−C−O angles of the formate ligands from the experimental and computational data, which reflects the rigidity of the ligand due to the sp^2 hybridization; ligand rigidity is also observed in MOF-5 and $[Cu(CO_3)_2][(CH_6N_3)_2]$.[29,31] Similarly, the O−Zn−O angles within the ZnO_6 octahedra do not vary significantly (Table S2, SI), though a rather small decrease in the Zn−O bond lengths, from 2.103(2) to 2.089(2) Å from ambient pressure to 0.94 GPa experimentally, is observed (Figures 5 and S2, SI). Similar changes in the Zn−O bond

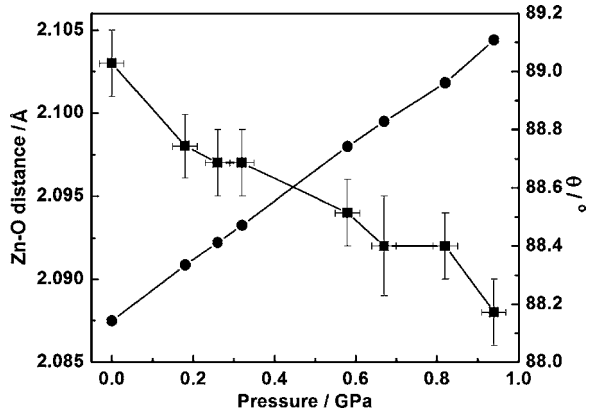

Figure 5. Evolution of the Zn−O distance (black squares with error bars) and θ (black circles) as a function of hydrostatic pressure.

distance upon hydrostatic compression were observed previously in a zinc phosphate phosphonoacetate hydrate, ZnPA, and MOF-5.[31,33] Though the Zn−O bond distances and lattice parameters obtained from our optimized computational model are slightly longer (on average, approximately 0.03 Å) than the experimental values in the range from ambient pressures to 1 GPa, the trends of all structural changes are consistent with the experimental data (Figures S2−S4, SI). The computed model was subjected to hydrostatic pressures as high as 4 GPa, where the subtle trends of structural changes observed in the 0−1 GPa range are intensified and become clearer (Figure S1 and Table S4, SI). Following the structural changes observed both experimentally and computationally, the NLC mechanism of framework **1** can be rationalized as follows. As seen in Figure 5, the Zn−O bond length decreases upon hydrostatic compression. In addition, tilting of the rigid formate ligands, occurring simultaneously with the Zn−O bond shortening, increases the angle θ facing the *c* axis from 88.14(1) to 89.11(1)° with increasing pressure (Figure S5, SI) and thus is directly responsible for the increase in the *c* axes. The ammonium cations are hydrogen bonded to the anionic framework and thus follow the structural changes of the framework to maintain optimal hydrogen bonding. Since each metal node is involved in both the four- and six-membered Zn−OCHO−Zn−OCHO rings, these rings change cooperatively in response to the external stimulus. This leads to the elongation and contraction of the orthogonal diagonals within the four-membered Zn−OCHO−Zn−OCHO rings, respectively. In line with the above, the *c*/*a* ratio changes significantly, from 1.118 to 1.137 at ambient pressure to 0.94 GPa experimentally and 1.151 to 1.169 at ambient pressure to 1 GPa computationally (Figure S6). The NLC behavior of framework **1** can be ascribed to a wine-rack mechanism of the type described by Baughman et al.[1] and shown in Figure 1d. It is noteworthy that framework **1** is purely assembled via the Zn−O coordination bonds; this simple framework structure therefore differs from the more anisotropic inorganic NLC wine-rack framework, $KMn[Ag(CN)_2]_3$, in which weakly bonded silver layers are interconnected via strong covalent bonds. Similarly, it is quite different from the organic NLC lattice fence system, methanol monohydrate, in which the hydrogen-bonded layers are linked via weak van der Waals interactions.[8]

In conclusion, a 3D zinc formate framework $[NH_4][Zn(HCOO)_3]$, possessing an *acs* topology, was discovered to show NLC along its *c* axis. High-pressure single-crystal X−ray diffraction and DFT calculations revealed the contraction of the Zn−O distances with increasing pressure combined with tilting of the formate ligands, resulting in the shrinkage along the *a* and *b* axes and the NLC effect along *c*. This work opens up an exciting new area for inorganic−organic framework materials with respect to rare functionality known only in classical inorganic and organic materials. Given the frequent occurrence of strong anisotropy in hybrid framework materials,[15a,34,35] this study suggests that NLC may turn out to be quite common in such systems.

■ ASSOCIATED CONTENT

Supporting Information

Experimental details, Tables S1−S4, Figures S1−S9, and CIF files. This material is available free of charge via the Internet at http://pubs.acs.org.

■ AUTHOR INFORMATION

Corresponding Author

akc30@cam.ac.uk; monica.kosa.shtaif@gmail.com

Notes

The authors declare no competing financial interest.

■ ACKNOWLEDGMENTS

W.L., T.D.B., A.T., R.P.B. and A.K.C. acknowledge the European Research Council for providing financial support. R.P.B. also thanks the Oppenheimer Fund for financial support. J.A.K.H. and M.R.P. thank the EPSRC for funding. W.L. also thanks Mr. Matthew Cliffe for help with the PASCal software and Prof. T. W. Clyne for access to the polishing facilities in the Gordon Laboratory.

■ REFERENCES

(1) Baughman, R. H.; Stafström, S.; Cui, C.; Dantas, S. O. *Science* **1998**, *279*, 1522.
(2) Goodwin, A. L.; Keen, D. A.; Tucker, M. G. *Proc. Natl. Acad. Sci. U.S.A.* **2010**, *107*, 9938.
(3) Grima, J. N.; Attard, D.; Caruana-Gaucib, R.; Gatt, R. *Scr. Mater.* **2011**, *65*, 565.
(4) Mariathasan, J. W. E.; Finger, L. W.; Hazen, R. M. *Acta Crystallogr., Sect. B* **1985**, *41*, 179.
(5) McCann, D. R.; Cartz, L.; Schmunk, R. E.; Harker, Y. D. *J. Appl. Phys.* **1972**, *43*, 1432.
(6) Haines, J.; Chateau, C.; Léger, J. M.; Bogicevic, C.; Hull, S.; Klug, D. D.; Tse, J. S. *Phys. Rev. Lett.* **2003**, *91*, 015503.
(7) Cairns, A. B.; Thompson, A. L.; Tucker, M. G.; Haines, J.; Goodwin, A. L. *J. Am. Chem. Soc.* **2012**, *134*, 4454.
(8) Fortes, A. D.; Suard, E.; Knight, K. S. *Science* **2011**, *331*, 742.
(9) (a) Cheetham, A. K.; Rao, C. N. R.; Feller, R. K. *Chem. Commun.* **2006**, 4780. (b) Rao, C. N. R.; Cheetham, A. K.; Thirumurugan, A. *J. Phys.: Condens. Matter* **2008**, *20*, 083202.
(10) O'Keeffe, M.; Yaghi, O. M. *Chem. Rev.* **2012**, *112*, 675.
(11) Férey, G. *Chem. Soc. Rev.* **2008**, *37*, 191.
(12) (a) Xu, G.-C.; Ma, X.-M.; Zhang, L.; Wang, Z.-M.; Gao, S. *J. Am. Chem. Soc.* **2010**, *132*, 9588. (b) Xu, G.-C.; Zhang, W.; Ma, X.-L.; Chen, Y.-H.; Zhang, L.; Cai, H.-L.; Wang, Z.-M.; Xiong, R.-G.; Gao, S. *J. Am. Chem. Soc.* **2011**, *133*, 14948. (c) Wang, Z.; Zhang, B.; Inoue, K.; Fujiwara, H.; Otsuka, T.; Kobayashi, H.; Kurmoo, M. *Inorg. Chem.* **2007**, *46*, 437.
(13) Sudik, A. C.; Côté, A. P.; Yaghi, O. M. *Inorg. Chem.* **2005**, *44*, 2998.
(14) Gong, J.; Miao, H.; Peng, Z. *Mater. Lett.* **2004**, *58*, 1349.
(15) (a) Kiran, M. S. R. N.; Varughese, S.; Reddy, C. M.; Ramamurty, U.; Desiraju, G. R. *Cryst. Growth Des.* **2010**, *10*, 4650. (b) Varughese, S.; Kiran, M. S. R. N.; Solanko, K. A.; Bond, A. D.; Ramamurty., U.; Desiraju, G. R. *Chem. Sci.* **2011**, *2*, 2236. (c) Kiran, M. S. R. N.; Varughese, S.; Ramamurty., U.; Desiraju, G. R. *CrystEngComm* **2012**, *14*, 2489.
(16) (a) Tan, J. C.; Merrill, C. A.; Orton, J. B.; Cheetham, A. K. *Acta Mater.* **2009**, *57*, 3481. (b) Tan, J. C.; Civalleri, B.; Lin, C. C.; Valenzano, L.; Galvelis, R.; Chen, P. F.; Bennett, T. D.; Mellot-Draznieks, C.; Zicovich-Wilson, C. M.; Cheetham, A. K. *Phys. Rev. Lett.* **2012**, *108*, 095502. (c) Tan, J. C.; Cheetham, A. K. *Chem. Soc. Rev.* **2011**, *40*, 1059.
(17) Tan, J.-C.; Jain, P.; Cheetham, A. K. *Dalton* **2012**, *41*, 3949.
(18) (a) Probert, M. R.; Robertson, C. M.; Coome, J. A.; Howard, J. A. K.; Michell, B. C.; Goeta, A. E. *J. Appl. Crystallogr.* **2010**, *43*, 1415. (b) Probert, M. R.; Chung, Y. H. P.; Howard, J. A. K. *CrystEngComm* **2010**, *12*, 2584.
(19) Piermarini, G. J.; Block, S.; Barnett, J. D.; Forman, R. A. *J. Appl. Phys.* **1975**, *46*, 2774.
(20) Angel, R. J.; Jackson, J. M.; Reichmann, H. J.; Speziale, S. *Eur. J. Mineral.* **2009**, *21*, 525.
(21) Angel, R. J. *High-Temperature and High-Pressure Crystal Chemistry, Mineralogical Society of America Geochemical Society*; Hazen, R. M., Downs, R. T., Eds.; Mineralogical Society of America: Chantilly, VA , **2000**; Vol. *41*, pp. 35−59.
(22) The least-squares fitting of *P*−*V* data with a Birch−Murnaghan equation of state were performed with the EOS-FIT software version 5.2, which is available at www.rossangel.net.
(23) Bennett, T. D.; Simoncic, P.; Moggach, S. A.; Gozzo, F.; Macchi, P.; Keen, D. A.; Tan, J.-C.; Cheetham, A. K. *Chem. Commun.* **2011**, *47*, 7893.
(24) Moggach, S. A.; Bennett, T. D.; Cheetham, A. K. *Angew. Chem., Int. Ed.* **2009**, *48*, 7087.
(25) Chapman, K. W.; Halder, G. J.; Chupas, P. J. *J. Am. Chem. Soc.* **2009**, *131*, 17546.
(26) Spencer, E. C.; Angel, R. J.; Ross, N. L.; Hanson, B. E.; Howard, J. A. K. *J. Am. Chem. Soc.* **2009**, *131*, 4022.
(27) Bennett, T. D.; Tan, J. C.; Moggach, S. A.; Galvelis, R.; Mellot-Draznieks, C.; Reisner, B. A.; Thirumurugan, A.; Allan, D. R.; Cheetham, A. K. *Chem.—Eur. J.* **2010**, *16*, 10684.
(28) Chapman, K. W.; Halder, G. J.; Chupas, P. J. *J. Am. Chem. Soc.* **2008**, *130*, 10524.
(29) Spencer, E. C.; Ross, N. L.; Angel, R. J. *J. Mater. Chem.* **2012**, *22*, 2074.
(30) The linear compressibilities were determined via error-weighted fits to the lattice parameters using an empirical expression of the form $l = l_0 + \lambda(p - p_c)^v$ and performed with PASCal software from http://pascal.chem.ox.ac.uk/.
(31) Graham, A. J.; Allan, D. R.; Muszkiewicz, A.; Morrison, C. A.; Moggach, S. A. *Angew. Chem., Int. Ed.* **2011**, *50*, 11138.
(32) Kornblatt, J. A. *Science* **1998**, *281*, 143.
(33) Kosa, M.; Tan, J.-C.; Merill, C. A.; Krack, M.; Cheetham, A. K.; Parrinello, M. *ChemPhysChem* **2010**, *11*, 2332.
(34) Li, W.; Barton, P. T.; Kiran, M. S. R. N.; Burwood, R. P.; Ramamurty, U.; Cheetham, A. K. *Chem.—Eur. J.* **2011**, *17*, 12429.
(35) Tan, J. C.; Furman, J. D.; Cheetham, A. K. *J. Am. Chem. Soc.* **2009**, *131*, 14252.